Pergamon

0045-7930(94)00031-X

Computers & Fluids Vol. 24, No. 3, pp. 209–225, 1995

0045-7930/95 $9.50 + 0.00

INVARIANT DISCRETIZATION OF THE k–ϵ MODEL IN GENERAL CO-ORDINATES FOR PREDICTION OF TURBULENT FLOW IN COMPLICATED GEOMETRIES

M. ZIJLEMA, A. SEGAL and P. WESSELING

Faculty of Technical Mathematics and Informatics, Delft University of Technology, P.O. Box 5031, 2600 GA Delft, The Netherlands

(Received 13 April 1994; in revised form 21 September 1994)

Abstract— An invariant formulation and finite volume discretization of the standard k–ϵ turbulence model in general curvilinear co-ordinates is presented. The k–ϵ model is implemented together with the incompressible Navier–Stokes equations on staggered grids with contravariant flux components as unknowns. A proof that k and ϵ are non-negative is given. Positive schemes in the implementation of the k–ϵ model are evaluated. Discretization of boundary conditions is considered. The numerical method is applied to a turbulent flow across a staggered tube bank.

1. INTRODUCTION

During the past decade a number of numerical methods have been proposed for the solution of the incompressible Reynolds-averaged Navier–Stokes equations in complicated geometries. Closure of these equations is effected by a turbulence model. Most publications (e.g. [1–5]) adopt a boundary-fitted curvilinear co-ordinate system and a k–ϵ model. In these articles various formulations (finite difference or finite volume, staggered or colocated grids, orthogonal or non-orthogonal co-ordinates, Cartesian or contravariant velocity components) are chosen for the development of the numerical method. A useful discussion of the advantages and disadvantages of the various possibilities can be found in [2] and [6].

In [7–10] a co-ordinate invariant finite volume discretization on a staggered non-orthogonal grid of the incompressible Navier–Stokes equations is presented. This discretization is formulated in standard tensor notation. As a consequence, the formulation contains Christoffel symbols, which involve second derivatives of the co-ordinate mapping. Hence, inaccurate discretizations may result on non-smooth grids. The main conclusions of these papers, however, are:

1. accurate results for 2D laminar flows were obtained on fairly smooth grids,
2. use of the contravariant flux components $V^\alpha = \sqrt{g}U^\alpha$, where $\sqrt{g}$ is the Jacobian of the co-ordinate mapping, as unknowns gives much better accuracy than the use of the contravariant velocity components U^α.

This paper extends this work to the turbulent case, presenting a co-ordinate invariant discretization of the standard high-Re k–ϵ model with wall functions [11] in boundary-fitted co-ordinates using tensor notation.

For physical reasons it is essential that the k–ϵ model yields non-negative values for the turbulent kinetic energy k and the dissipation rate of turbulent energy ϵ. To the authors' knowledge, a proof that the k–ϵ model has this property is not available. In this paper we shall prove that the model with certain boundary conditions has only non-negative solutions.

The discretized turbulence equations should also possess the positivity property. Numerical experiments have shown that negative values of k and ϵ are detrimental to the stability of the k–ϵ model. Several measures have been proposed to enhance numerical stability [12–16]. For example, the convective transport terms are often approximated with a highly stable low-order scheme, which unfortunately can introduce numerical diffusion and hence high levels of numerical errors. However, it is not possible to construct an accurate, non-diffusive scheme that produces unconditionally non-negative solutions, especially on highly non-orthogonal grids. But false diffusion should be kept to a minimum.

The outline of this paper is as follows. In Section 2 the incompressible Navier–Stokes equations and the high-Re k–ϵ model are presented in tensor formulation. We prove that under certain conditions this model has only non-negative solutions. In Section 3 we focus attention to the discretization of the k–ϵ equations for instationary turbulent flows in two dimensions by the finite volume method. Positive difference schemes are treated. Discretization of the boundary conditions often receives less attention than the discretization of the differential equations themselves, but this is unwarranted. For that reason, details about the implementation of Dirichlet and Neumann boundary conditions are given. In Section 4 the time discretization and a solution method are briefly considered. Finally, in Section 5 we present an application of the method to a complicated turbulent flow, namely turbulent flow through a sub-channel of staggered tube bundles.

2. TENSOR FORMULATION OF GOVERNING EQUATIONS

Many turbulent flows of practical interest are bounded by curved surfaces. To compute such flows a boundary-fitted curvilinear co-ordinate system may be introduced. Consequently, the partial differential equations governing incompressible turbulent flows must be transformed to this co-ordinate system. For formulating the equations in general co-ordinates tensor notation is almost indispensable. The essentials of tensor analysis can be found e.g. in [17, 18]. In this section we summarize some basic facts. We restrict ourselves to the two-dimensional case.

The physical domain Ω is mapped onto a rectangular computational domain G. It is assumed that the mapping $\mathbf{x} = \mathbf{x}(\boldsymbol{\xi}): G \to \Omega$ is regular, i.e. the Jacobian J of the transformation does not vanish; $\mathbf{x}$ are Cartesian co-ordinates and $\boldsymbol{\xi}$ are boundary conforming curvilinear co-ordinates.

The covariant and contravariant base vectors of the curvilinear co-ordinate system $\mathbf{a}_{(\alpha)}$ and $\mathbf{a}^{(\alpha)}$, respectively, are defined as follows:

$$\mathbf{a}_{(\alpha)} = \frac{\partial \mathbf{x}}{\partial \xi^{(\alpha)}}, \quad \mathbf{a}^{(\alpha)} = \frac{\partial \xi^{\alpha}}{\partial \mathbf{x}} \tag{1}$$

The covariant base vector $\mathbf{a}_{(\alpha)}$ is tangential to the co-ordinate lines $\xi^{\alpha} = \textit{constant}$, whereas $\mathbf{a}^{(\alpha)}$ is perpendicular to the surfaces on which ξ^{α} is constant.

The covariant and contravariant metric tensors $g_{\alpha\beta}$ and $g^{\alpha\beta}$ are defined by

$$g_{\alpha\beta} = \mathbf{a}_{(\alpha)} \cdot \mathbf{a}_{(\beta)}, \quad g^{\alpha\beta} = \mathbf{a}^{(\alpha)} \cdot \mathbf{a}^{(\beta)} \tag{2}$$

The square root of the determinant of the covariant metric tensor equals the Jacobian of the transformation, given by

$$\sqrt{g} = J = \mathbf{a}_{(1)} \cdot (\mathbf{a}_{(2)} \wedge \mathbf{a}_{(3)}) \tag{3}$$

Assuming right-handed co-ordinate systems $\boldsymbol{x}$ and $\boldsymbol{\xi}$, $J > 0$.

A covariant derivative is a tensor which reduces to a partial derivative of a tensor field in Cartesian co-ordinates. For a tensor of rank zero ϕ, the covariant derivative is the same as the partial derivative, and is denoted by

$$\phi_{,\alpha} \equiv \frac{\partial \phi}{\partial \xi^{\alpha}} \tag{4}$$

It can be shown that a covariant derivative of a tensor of rank one and a covariant derivative of a tensor of rank two are given by

$$U^{\alpha}_{,\beta} = \frac{\partial U^{\alpha}}{\partial \xi^{\beta}} + \begin{Bmatrix} \alpha \\ \gamma\beta \end{Bmatrix} U^{\gamma} \tag{5}$$

$$T^{\alpha\beta}_{,\beta} = \frac{1}{\sqrt{g}} \frac{\partial \sqrt{g} T^{\alpha\beta}}{\partial \xi^{\beta}} + \begin{Bmatrix} \alpha \\ \gamma\beta \end{Bmatrix} T^{\gamma\beta} \tag{6}$$

where

$$\begin{Bmatrix} \alpha \\ \gamma\beta \end{Bmatrix} = \mathbf{a}^{(\alpha)} \cdot \frac{\partial \mathbf{a}_{(\beta)}}{\partial \xi^{\gamma}} = \frac{\partial \xi^{\alpha}}{\partial x^{\delta}} \cdot \frac{\partial^2 x^{\delta}}{\partial \xi^{\gamma} \partial \xi^{\beta}} = \begin{Bmatrix} \alpha \\ \beta\gamma \end{Bmatrix} \tag{7}$$

is the Christoffel symbol of the second kind. The summation convention holds for Greek indices.

The incompressible Reynolds-averaged Navier–Stokes equations in general co-ordinates are given by

$$U^{\alpha}_{,\alpha} = 0 \tag{8}$$

$$\frac{\partial U^{\alpha}}{\partial t} + (U^{\alpha}U^{\beta})_{,\beta} + (g^{\alpha\beta}p)_{,\beta} - \tau^{\alpha\beta}_{,\beta} = F^{\alpha} \tag{9}$$

Here, U^{α} is the contravariant mean velocity component, p is the pressure, F^{α} is an external force per unit volume and $\tau^{\alpha\beta}$ contains viscous and Reynolds stress tensors and is given by

$$\tau^{\alpha\beta} = (\nu + \nu_t)(g^{\alpha\gamma}U^{\beta}_{,\gamma} + g^{\beta\gamma}U^{\alpha}_{,\gamma}) \tag{10}$$

where ν is the kinematic viscosity and ν_t is the isotropic eddy-viscosity which is given by

$$\nu_t = c_{\mu}\frac{k^2}{\epsilon} \tag{11}$$

Here, k is the turbulent kinetic energy per unit mass and ϵ is the turbulent energy dissipation rate per unit mass, defined as

$$k = \tfrac{1}{2}\,\overline{\hat{U}^{\alpha}\hat{U}_{\alpha}} \tag{12}$$

$$\epsilon = \nu g^{\beta\gamma}\,\overline{\hat{U}^{\alpha}_{,\gamma}\hat{U}_{\alpha,\beta}} \tag{13}$$

where $\hat{U}^{\alpha}$ and $\hat{U}_{\alpha}$ are the contravariant and covariant components of the velocity fluctuations, respectively. The turbulence quantities k and ϵ are obtained from modeled transport equations which read, in general curvilinear co-ordinates:

$$\frac{\partial k}{\partial t} + (U^{\alpha}k)_{,\alpha} - \left(\frac{\nu_t}{\sigma_k}g^{\alpha\beta}k_{,\beta}\right)_{,\alpha} = P_k - \epsilon \tag{14}$$

$$\frac{\partial \epsilon}{\partial t} + (U^{\alpha}\epsilon)_{,\alpha} - \left(\frac{\nu_t}{\sigma_{\epsilon}}g^{\alpha\beta}\epsilon_{,\beta}\right)_{,\alpha} = \frac{\epsilon}{k}(c_{\epsilon 1}P_k - c_{\epsilon 2}\epsilon) \tag{15}$$

P_k is the production of turbulent kinetic energy, given by

$$P_k = \nu_t g_{\alpha\delta}(g^{\alpha\gamma}U^{\beta}_{,\gamma} + g^{\beta\gamma}U^{\alpha}_{,\gamma})U^{\delta}_{,\beta} \tag{16}$$

Finally, c_{μ}, $c_{\epsilon 1}$, $c_{\epsilon 2}$, σ_k and σ_{ϵ} are dimensionless constants which, respectively, are taken to be 0.09, 1.44, 1.92, 1.0 and 1.3 (following [11]).

The transport equations (14) and (15) have been modeled, which means that some unknown terms in the exact transport equations for k and ϵ have been approximated in terms of quantities that we can determine. The modeled transport equations should not be capable of producing negative values of k and ϵ, because of the definitions of these quantities [cf. (12) and (13)]. Such a model is said to be realizable.

Unlike the Reynolds-stress closures, not much attention has been paid to the realizability of the k–ϵ modelling in the literature. Cardot *et al.* [19] claimed that if the k–ϵ model has a smooth solution for given positive initial and Dirichlet conditions, then k and ϵ stay positive at later times. However, it is not clear how they support this claim.

We shall now show that the k–ϵ model has non-negative solutions at all times for any positive initial conditions, positive Dirichlet and homogeneous Neumann boundary conditions, if the empirical constant $c_{\epsilon 2} > 1$. We assume that the solutions k and ϵ are sufficiently smooth. Let t_0 be the first time that there exists a $\xi_m \in G$ such that $k(\xi_m, t_0) = 0$. Because the Dirichlet boundary conditions on k is positive, it is necessary that $\xi_m \in G \backslash \partial G_D$, where ∂G_D is the Dirichlet boundary. If ξ_m is the interior, then at (ξ_m, t_0) the gradient of k is zero, because we have a minimum. This is also true when ξ_m lies on a Neumann boundary, because the normal component of the gradient of k is zero. Furthermore, it can be shown that the time scale of turbulence $\Theta \equiv k/\epsilon$ is strictly positive, $\forall t \geqslant 0$ and $\forall \xi \in G$, if $c_{\epsilon 2} > 1$. The proof is given in the Appendix. Thus, we have

$$\nu_t = c_{\mu}\frac{k^2}{\epsilon} = c_{\mu}k\Theta = 0 \quad \text{at } t = t_0 \tag{17}$$

By writing out the diffusion term one sees that

$$\left(\frac{\nu_t}{\sigma_k} g^{\alpha\beta} k_{,\beta}\right)_{,\alpha} = \frac{g^{\alpha\beta}}{\sigma_k}(k_{,\beta}\nu_{t,\alpha} + \nu_t k_{,\alpha\beta}) = 0 \quad \text{at } t = t_0 \tag{18}$$

From (16) and (17) it is clear that the production of turbulent kinetic energy is zero at $t = t_0$ in ξ_m. Hence, the equation (14) reduces to $\partial k/\partial t = -\epsilon$. Because k is decreasing at (ξ_m, t_0), $\partial k/\partial t$ must be negative or zero. Therefore, $\epsilon \geqslant 0$. Moreover, $k = 0$ and $k/\epsilon > 0$. Hence, the only way to avoid a contradiction is to have $\epsilon = 0$, and we conclude that $\partial k/\partial t = 0$. So, if k vanishes, its time derivative also vanishes. Furthermore, it can be shown by taking the time derivative of left- and right-hand sides of equation (14) and using the fact that $k = k_{,\alpha} = \partial k/\partial t = 0$ that $\partial^2 k/\partial t^2 > 0$ at $t = t_0$ in ξ_m. We conclude that $k = 0$ is a local minimum and therefore, the turbulent kinetic energy cannot become negative. From the fact that $\forall t \geqslant 0 : k \geqslant 0$ and $k/\epsilon > 0$, it is clear that $\epsilon \geqslant 0$, $\forall t \geqslant 0$.

A discussion of the specification of boundary conditions for the momentum equations can be found in [9]. Additionally, in the case of turbulent flows, in near-wall regions wall functions (described by Launder and Spalding [11]) are used in order to avoid integration through the viscous sublayer and to obtain a logarithmic velocity profile:

$$\tau_w = \frac{c_\mu^{1/4}\kappa\sqrt{k_P}}{\ln(EY_P^+)}\mathbf{u}\cdot\mathbf{t}_P \tag{19}$$

where

$$Y_P^+ \equiv \frac{c_\mu^{1/4} Y_P \sqrt{k_P}}{\nu} \tag{20}$$

Here, κ is the Von Kármán constant (≈ 0.4) and E is a roughness parameter, approximately equal to 9.0 for a smooth wall. The subscript P refers to the center of a cell adjacent to the wall. The location of the first grid point away from the wall must be such that $Y_P^+ > 11.3$ in which the wall-law (19) is valid. The tangential velocity along the wall expressed in terms of contravariant components reads:

$$\mathbf{u}\cdot\mathbf{t} = \frac{g_{t\alpha}}{\sqrt{g_{tt}}} U^\alpha, \quad t = 1 \text{ or } 2 \tag{21}$$

Finally, the normal distance Y_P is evaluated as follows, see Fig. 1:

$$Y_P = \tfrac{1}{2}\mathbf{AB}\cdot\mathbf{n} = \frac{\mathbf{AB}\cdot\mathbf{a}^{(n)}}{2\sqrt{g^{nn}}}, \quad n = 1 \text{ or } 2 \tag{22}$$

where **A** and **B** are some points on cell faces whose co-ordinates can be obtained by linear interpolation from the co-ordinates of cell vertices, which are assumed to be given.

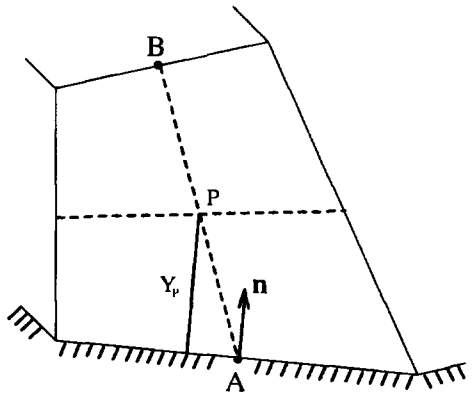

Fig. 1. Calculation of distance between near wall point and the wall.

In order to account for near-wall effects on the turbulent energy, the production of turbulent kinetic energy in the first grid point away from the wall is approximated by

$$P_k = \tau_w \frac{\mathbf{u}\cdot\mathbf{t}_P}{Y_P} \tag{23}$$

whereas the dissipation rate of turbulent energy is evaluated as follows:

$$\epsilon = c_\mu^{3/4} k_P^{3/2} \frac{\ln(EY_P^+)}{\kappa Y_P} \tag{24}$$

Finally, the flux of k through the wall is set to zero and ϵ is given in point P by

$$\epsilon = \frac{c_\mu^{3/4} k_P^{3/2}}{\kappa Y_P} \tag{25}$$

3. FINITE VOLUME DISCRETIZATION OF TURBULENCE EQUATIONS

Equations (14) and (15) are convection-diffusion equations with source terms. Hence, for their discretization the following equation will be considered in the remainder of this paper:

$$\frac{\partial \phi}{\partial t} + (U^\alpha \phi)_{,\alpha} - (K^{\alpha\beta}\phi_{,\beta})_{,\alpha} = S_\phi \tag{26}$$

where ϕ denotes a scalar and S_ϕ a source term which depends on ϕ and U^α. Furthermore, $K^{\alpha\beta} = \kappa g^{\alpha\beta}$ with κ a diffusion coefficient. It is assumed that both source term and diffusion coefficient are sufficiently smooth.

As mentioned in the previous section, the physical domain Ω is transformed to a rectangle G in which a uniformed grid G_h is defined. It is assumed that only co-ordinates $\mathbf{x}(\xi)$ of the vertices of the cells are known. A staggered grid is used. Figure 2 shows a part of the staggered grid in the computational plane. Scalars ϕ are given in the cell centers and U^α is given in centers of cell faces connecting vertices with equal values of ξ^α.

In the following section we consider the space discretization by means of the finite volume method of each term in (26) separately. It is an essential requirement that a numerical scheme for the turbulence equations yield non-negative values of k and ϵ. An important reason to require this is that several numerical experiments have shown that negative values of k and ϵ tend to be amplified and can destabilize the computations by nonlinearities and coupling. Suppose that discretization of (26) (without source term) results in

$$a_{i,j}^{00}\phi_{i,j}^{n+1} = \sum_{k,l\neq 0} a_{i,j}^{kl}\phi_{i+k,j+l}^{n+1} + \phi_{i,j}^{n} \tag{27}$$

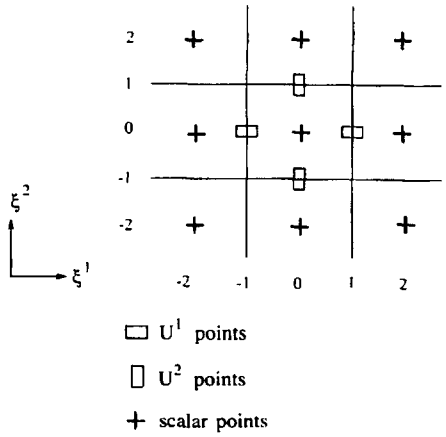

Fig. 2. Arrangement of the unknowns for a staggered grid.

with

$$a_{i,j}^{00} = 1 + \sum_{k,l \neq 0} a_{i,j}^{kl} \tag{28}$$

for all points (i, j) in the computational grid G_h. It can be shown that unconditionally positive solutions will result if $a_{i,j}^{00} > 0$ and $\forall k \neq 0$, $\forall l \neq 0$: $a_{i,j}^{kl} \geq 0$. A scheme (27) satisfying these sufficient conditions is said to be positive or monotone. With respect to the accuracy of a positive scheme, it can be shown by Taylor series expansion that this scheme is at best first order accurate, unless the grid is orthogonal and mesh-Péclet numbers are smaller than 2, as will be seen later in the next section. In that case the scheme can be both second order accurate and positive.

3.1. Discretization in the interior

For convenience we introduce the local cell co-ordinates given by Fig. 2. The mapping $\mathbf{x} = \mathbf{x}(\xi)$ is chosen such that $\Delta\xi^1 = \Delta\xi^2 = 1$.

The diffusion term

Integration over a finite volume Ω with center (0, 0) gives, using the Gauss divergence theorem

$$-\int_\Omega (K^{\alpha\beta}\phi_{,\beta})_{,\alpha}\,\mathrm{d}\Omega = -\int_{\partial\Omega} K^{\alpha\beta}\frac{\partial\phi}{\partial\xi^\beta}\,\mathrm{d}\Gamma_\alpha \approx -\sqrt{g}K^{1\beta}\frac{\partial\phi}{\partial\xi^\beta}\bigg|_{(-1,0)}^{(1,0)} - \sqrt{g}K^{2\beta}\frac{\partial\phi}{\partial\xi^\beta}\bigg|_{(0,-1)}^{(0,1)} \tag{29}$$

The right-hand side of (29) has to be approximated further. This is done by central differences. For example

$$\frac{\partial\phi}{\partial\xi}\bigg|_{(1,0)} \approx \phi_{(2,0)} - \phi_{(0,0)} \tag{30}$$

It is clear that this approximation contributes to a positive scheme. However, this is not true for terms associated with mixed derivatives ($K^{12} = \kappa g^{12} \neq 0$). For example, if we approximate $\partial\phi/\partial\xi^2|_{(1,0)}$ by central differences and bilinear (4-point) interpolations

$$\frac{\partial\phi}{\partial\xi^2}\bigg|_{(1,0)} \approx \tfrac{1}{4}(\phi_{(0,2)} + \phi_{(2,2)} - \phi_{(0,-2)} - \phi_{(2,-2)}) \tag{31}$$

then the coefficients corresponding to $\phi_{(0,-2)}$ and $\phi_{(2,-2)}$ get the wrong sign, if $g^{12} > 0$. On the other hand, if $g^{12} < 0$ then the coefficients corresponding to $\phi_{(0,2)}$ and $\phi_{(2,2)}$ will get the wrong sign. However, these coefficients are usually small relative to other coefficients, but, in some circumstances, for example when the grid is highly non-orthogonal, they become significant. For that reason many authors (e.g. [5, 6, 12, 14, 16]) treat the mixed derivative explicitly, evaluating it at the previous time level. This method does not lower the accuracy of the scheme in the steady state case, but may affect its convergence rate. This method is most frequently used. Schemes for approximation of mixed derivatives which produce non-negative coefficients were also evaluated. One of these schemes, proposed in [12], is based on 2-point rather than 4-point interpolation. For example, suppose that $g^{12} > 0$, then the following approximation is made:

$$\frac{\partial\phi}{\partial\xi^2}\bigg|_{(1,0)} \approx \phi_{(1,1)} - \phi_{(1,-1)} = \tfrac{1}{2}(\phi_{(0,0)} + \phi_{(2,2)} - \tfrac{1}{2}(\phi_{(0,-2)} + \phi_{(2,0)}) \tag{32}$$

Similarly, if $g^{12} < 0$

$$\frac{\partial\phi}{\partial\xi^2}\bigg|_{(1,0)} \approx \tfrac{1}{2}(\phi_{(0,2)} + \phi_{(2,0)} - \phi_{(0,0)} - \phi_{(2,-2)}) \tag{33}$$

This scheme produces unconditionally non-negative coefficients of the nodes corresponding to points $(-2, -2)$, $(2, 2)$, $(2, -2)$ and $(-2, 2)$. However, this is not true for the nodes corresponding to points $(0, -2)$, $(-2, 0)$, $(2, 0)$ and $(0, 2)$. It can be shown that these coefficients will stay non-negative if the following condition is satisfied

$$|g^{12}| \leq \min(g^{11}, g^{22}) \tag{34}$$

provided that the diffusion coefficient κ is locally uniform and the metric tensors g^{12} at center of each of cell-faces are approximately equal. Another example is a scheme, which uses one-sided rather than central differences. This gives, taking a cell face with center at (1, 0) as an example

$$\left.\frac{\partial\phi}{\partial\xi^2}\right|_{(1,0)} \approx \tfrac{1}{2}\phi_{(2,2)} + \tfrac{1}{2}\phi_{(0,2)} - \phi_{(0,0)} \quad \text{if } g^{12} > 0 \tag{35}$$

or

$$\left.\frac{\partial\phi}{\partial\xi^2}\right|_{(1,0)} \approx \phi_{(0,0)} - \tfrac{1}{2}\phi_{(2,-2)} - \tfrac{1}{2}\phi_{(0,-2)} \quad \text{if } g^{12} < 0 \tag{36}$$

Obviously, this decreases the accuracy to order one, but the scheme is unconditionally positive. Nevertheless, in many turbulent flows the turbulence quantities k and ϵ are often dominated by source terms and hence the mixed derivatives are of minor importance.

The convection term

Integration over a finite volume Ω with center (0, 0) gives

$$\int_\Omega (U^\alpha\phi)_{,\alpha}\,\mathrm{d}\Omega = \int_{\partial\Omega} U^\alpha\phi\,\mathrm{d}\Gamma_\alpha \approx V^1\phi|_{(-1,0)}^{(1,0)} + V^2\phi|_{(0,-1)}^{(0,1)} \tag{37}$$

where $V^\alpha = \sqrt{g}U^\alpha$. Since ϕ is only given in the center of a cell, further approximation is needed. Consider only the first part of the right-hand side of (37). The second part will be treated in the same way. Because of the fact that in many turbulent flow situations the mesh-Péclet number is several higher than order of one, positive schemes are needed to approximate the face values ϕ. In numerous publications the well-known hybrid central/upwind scheme [20] has been adopted. The approximations to the face values are then given by

$$\phi_{(1,0)} = \{1 - s(\mathrm{Pe}^1_{(1,0)})\}\phi_C|_{(1,0)} + s(\mathrm{Pe}^1_{(1,0)})\phi_U|_{(1,0)} \tag{38}$$

$$\phi_{(-1,0)} = \{1 - s(\mathrm{Pe}^1_{(-1,0)})\}\phi_C|_{(-1,0)} + s(\mathrm{Pe}^1_{(-1,0)})\phi_U|_{(-1,0)} \tag{39}$$

where $\phi_C|_{(k,0)}$ is given by

$$\phi_C|_{(k,0)} = \tfrac{1}{2}(\phi_{(k-1,0)} + \phi_{(k+1,0)}) \tag{40}$$

and $\phi_U|_{(k,0)}$ by

$$\phi_U|_{(k,0)} = \tfrac{1}{2}\{1 + \mathrm{sign}(V^1_{(k,0)})\}\phi_{(k-1,0)} + \tfrac{1}{2}\{1 - \mathrm{sign}(V^1_{(k,0)})\}\phi_{(k+1,0)} \tag{41}$$

where $k = \pm 1$. The mesh-Péclet number $\mathrm{Pe}^\alpha_{(k,l)}$ is defined by

$$\mathrm{Pe}^\alpha_{(k,l)} = \frac{V^\alpha_{(k,l)}}{2\{\sqrt{g_{(k,l)}}K^{\alpha\alpha}_{(k,l)} + \tfrac{1}{4}(\sqrt{g_{(l,k)}}K^{\beta\alpha}_{(l,k)} - \sqrt{g_{(-l,-k)}}K^{\beta\alpha}_{(-l,-k)})\}}, \quad \beta \neq \alpha \tag{42}$$

(no summation over α)

Here, $k, l \in \{-1, 0, 1\}$. For convergence reasons, the switching function $s(\mathrm{Pe})$ is defined as follows

$$s(\mathrm{Pe}) = 1 - \min\left\{1, \frac{1}{|\mathrm{Pe}|}\right\} \tag{43}$$

This switching function is obtained by requiring that off-diagonal matrix elements corresponding to convection and diffusion terms are non-positive.

In many 2D flow problems, the grid lines are not aligned with streamlines. As a consequence excessive numerical cross-flow diffusion occurs with the hybrid scheme. Moreover, in convection dominated flows the result of the hybrid scheme is that first-order upwind scheme is employed everywhere, irrespective of whether positiveness problems arise or not. In fact, most higher-order non-monotone schemes produces wiggles only in regions where steep gradients of turbulence quantities occur. There are many alternatives to developed higher-order monotone schemes. An

overview can be found in [21]. In the present paper a TVD/MUSCL scheme with the 'minmod' limiter is applied to approximate the convective turbulence transport accurately. The approximation of the face value ϕ at point (1, 0), for example, is given by

$$\phi_{(1,0)} = \phi_{(0,0)} + \tfrac{1}{2}\,\mathrm{minmod}(\phi_{(0,0)} - \phi_{(-2,0)}, \phi_{(2,0)} - \phi_{(0,0)}) \quad \text{if } V^1_{(1,0)} \geq 0 \tag{44}$$

$$\phi_{(1,0)} = \phi_{(2,0)} - \tfrac{1}{2}\,\mathrm{minmod}(\phi_{(4,0)} - \phi_{(2,0)}, \phi_{(2,0)} - \phi_{(0,0)}) \quad \text{if } V^1_{(1,0)} < 0 \tag{45}$$

where

$$\mathrm{minmod}(p, q) = \mathrm{sign}(p)\max\{0, \min[|p|, q\ \mathrm{sign}(p)]\} \tag{46}$$

For further details we refer to [22]. Because the limiter is nonlinear, this TVD/MUSCL scheme is implemented in a deferred correction manner:

$$\phi^{n+1}_{(1,0)} = \phi^{U,n+1}_{(1,0)} + (\phi^{T,n}_{(1,0)} - \phi^{U,n}_{(1,0)}) \tag{47}$$

where n represents the time level and "U" and "T" indicate a first-order upwind and TVD/MUSCL scheme, respectively.

The source term and the time derivative

The source term and the time derivative of ϕ in equation (26) are approximated by the midpoint rule in the following manner

$$\int_\Omega S_\phi \,\mathrm{d}\Omega \approx \sqrt{g}_{(0,0)} S_{\phi_{(0,0)}} \tag{48}$$

and

$$\int_\Omega \frac{\partial \phi}{\partial t}\,\mathrm{d}\Omega \approx \sqrt{g}_{(0,0)} \left.\frac{\partial \phi}{\partial t}\right|_{(0,0)} \tag{49}$$

One of the source terms is the production of turbulent energy (16) which must be evaluated. The discretization of this term is carried out at the centre of a scalar cell with central differencing. Since we use $V^\alpha = \sqrt{g}U^\alpha$ as unknowns, the covariant derivative of the contravariant velocity components must be expressed in terms of flux components. Using tensor analysis one can show that the following formula holds:

$$U^\alpha_{,\beta} = \frac{1}{\sqrt{g}}\left(\frac{\partial V^\alpha}{\partial \xi^\beta} - \left\{\begin{matrix}\gamma \\ \gamma\beta\end{matrix}\right\} V^\alpha + \left\{\begin{matrix}\alpha \\ \beta\gamma\end{matrix}\right\} V^\gamma\right) \tag{50}$$

Hence, the production term contains Christoffel symbols which do not allow us to use non-smooth grids. But experience shows that the approximation of this term gives good results on fairly smooth grids.

3.2. The boundary conditions

In this section we consider the implementation of the boundary conditions, which is crucial for the final solution. Because the equation (26) is elliptic, boundary conditions must be specified at all boundaries. At inlets, values of turbulence quantities, which are essentially non-negative, are specified. At outlets, zero normal gradient conditions for turbulence quantities may be imposed. The same holds for symmetry boundaries. At walls, wall functions, which consist of Dirichlet and homogeneous Neumann conditions, are applied. Hence, we consider both Dirichlet and homogeneous Neumann boundary conditions:

$$\phi \text{ given} \quad \text{and} \quad \frac{\partial \phi}{\partial \mathbf{n}} = 0 \tag{51}$$

Here, $\mathbf{n}$ denotes the outward normal to $\partial\Omega$. The implementation of these boundary conditions must be such that it results in a positive scheme.

We restrict ourselves to the left boundary of Ω, i.e. $\xi^1 = 0$. The other boundaries can be treated in exactly the same way. Again, the diffusion and convection terms of (26) will be handled separately.

The diffusion term

Suppose we have a Dirichlet boundary condition $\phi = g_D > 0$ at $\xi^1 = 0$. Then the following approximations are made:

$$\sqrt{g}K^{11}\frac{\partial\phi}{\partial\xi^1}\bigg|_{(-1,0)} \approx 2\sqrt{g}K^{11}|_{(-1,0)}(\phi_{(0,0)} - g_{D(-1,0)}) \tag{52}$$

and

$$\sqrt{g}K^{12}\frac{\partial\phi}{\partial\xi^2}\bigg|_{(-1,0)} \approx \sqrt{g}K^{12}|_{(-1,0)}(g_{D(-1,1)} - g_{D(-1,-1)}) \tag{53}$$

In (52) we use one-sided differences, while in (53) central differences are used. From (52), it is clear that the coefficient of $\phi_{(0,0)}$ is positive. Equation (53) contains only known terms and does not influence the positivity of the scheme.

In the case of the homogeneous Neumann boundary condition at $\xi^1 = 0$ we have

$$\kappa\frac{\partial\phi}{\partial\mathbf{n}} = -\frac{K^{1\beta}}{\sqrt{g^{11}}}\frac{\partial\phi}{\partial\xi^\beta} = 0 \tag{54}$$

Hence, the finite volume integration of the diffusion term of (26) becomes

$$-\int_\Omega (K^{\alpha\beta}\phi_{,\beta})_{,\alpha}\,\mathrm{d}\Omega \approx -\sqrt{g}K^{1\beta}\frac{\partial\phi}{\partial\xi^\beta}\bigg|_{(1,0)} - \sqrt{g}K^{2\beta}\frac{\partial\phi}{\partial\xi^\beta}\bigg|_{(0,1)} + \sqrt{g}K^{2\beta}\frac{\partial\phi}{\partial\xi^\beta}\bigg|_{(0,-1)} \tag{55}$$

where the local numbering of Fig. 2 is used. The terms of the right-hand side of (55) can be approximated in exactly the same way as in the previous section. However, this approximation introduces two virtual unknowns at the points $(-2, 0)$ and $(-2, 2)$ or $(-2, -2)$ depends on the sign of g^{12}. These virtual unknowns can be eliminated by means of the Neumann condition. For example, $\phi_{(-2,0)}$ can be eliminated as follows

$$\phi_{(-2,0)} = \phi_{(0,0)} \tag{56}$$

It is clear that this approximation produces a positive scheme, because the coefficient of $\phi_{(-2,0)}$ is negative, and with (28) the coefficient of $\phi_{(0,0)}$ becomes therefore positive.

The convection term

The upwind schemes, as treated in the previous section, introduce just one virtual unknown near a boundary. In the case of the left boundary this virtual unknown is $\phi_{(-2,0)}$, where the local numbering of Fig. 2 is used. With both Dirichlet and homogeneous Neumann conditions this virtual unknown can be eliminated using linear extrapolation. In the case of a Dirichlet boundary condition $\phi_{(-2,0)}$ can be eliminated by

$$\phi_{(-2,0)} = 2g_{D(-1,0)} - \phi_{(0,0)} \tag{57}$$

Because the coefficient of $\phi_{(-2,0)}$ is negative, the contribution to the coefficient of $\phi_{(0,0)}$ is positive. If we have the homogeneous Neumann boundary condition then (56) is used to eliminate $\phi_{(-2,0)}$.

4. TIME DISCRETIZATION AND SOLUTION METHOD

The spatial discretization of the convection–diffusion equation with source term (26), explained in the previous section, yields a system of ordinary differential equations of the following form

$$\frac{\mathrm{d}\boldsymbol{\phi}}{\mathrm{d}t} + T(\mathbf{V})\boldsymbol{\phi} = \mathbf{F} + \mathbf{S}_\phi \tag{58}$$

where $\mathbf{V}$ and $\boldsymbol{\phi}$ denote algebraic vectors containing the velocity and scalar unknowns, respectively. T represents the discretization of convection and diffusion terms, $\mathbf{F}$ contains the right-hand side term arising from the boundary conditions and $\mathbf{S}_\phi$ represents the source term and is nonlinear. Time discretization takes place with the so-called θ-method:

$$\frac{\boldsymbol{\phi}^{n+1} - \boldsymbol{\phi}^n}{\Delta t} + \theta T\boldsymbol{\phi}^{n+1} + (1-\theta)T\boldsymbol{\phi}^n = \mathbf{F} + \theta\mathbf{S}_\phi^{n+1} + (1-\theta)\mathbf{S}_\phi^n \tag{59}$$

where n denotes the preceding time level and $n+1$ the new time level. For $\theta = 1$ we obtain the first-order implicit Euler scheme, for $\theta = \frac{1}{2}$ the second-order Crank–Nicolson scheme, which is required for calculation of an unsteady turbulent flow. In order to solve the system of equations (59) the standard Newton linearization of the source term is used:

$$\mathbf{S}_\phi^{n+1} \approx \mathbf{S}_\phi^n + \frac{\partial \mathbf{S}_\phi^n}{\partial \boldsymbol{\phi}} (\boldsymbol{\phi}^{n+1} - \boldsymbol{\phi}^n) \tag{60}$$

For both the k and ϵ equations the following inequalities hold:

$$\mathbf{S}_\varphi^n \geqslant 0 \quad \text{and} \quad \frac{\partial \mathbf{S}_\phi^n}{\partial \boldsymbol{\phi}} < 0 \tag{61}$$

which preserves the positivity of the solutions. Here, we have assumed that the eddy-viscosity ν_t (occurring in the production term) has been frozen at time level n.

The system of linear equations is solved by an iterative GMRES method [23] with preconditioning. This method is very suitable for non-symmetric matrices and has a relatively good rate of convergence. More details can be found in [24].

The spatial and temporal discretizations of the incompressible Navier–Stokes equations are described in [9]. It should be noted that the convection terms in the momentum equations are approximated with central differencing. To ensure a divergence-free velocity field a second order pressure-correction method as described by Van Kan [25] is used. To solve the nonlinear system of equations we use the Newton linearization with the iterative GMRES method. After solving the continuity equation and the momentum equations, the equations for k and ϵ are solved in a decoupled way, as described before.

5. AN APPLICATION

Turbulent flow across a bank of staggered tubes is very interesting because of practical importance in the context of heat exchangers. From physical point of view, this flow type is more challenging, because the flow across tubes is undergoing stagnation, acceleration and separation. Ideally, a turbulence model in complex geometries should be able to respond correctly to those features. Therefore, the experimental arrangement of Simonin and Barcouda [26], as shown in Fig. 3, was set up as a testcase in the Second ERCOFTAC-IAHR Workshop on Refined Flow Modelling organized by UMIST in Manchester in 1993. Results obtained by various calculation methods, including the present one, can be found in [27].

It may be assumed that the flow in a region relatively far from the entrance becomes fully periodic and steady. Therefore, we focused on a sub-channel, identified as the shaded area in Fig. 3, in which the flow repeats itself in an anti-symmetrically manner. The diameter of the tube is $D = 21.7$ mm, the transverse pitch is taken to be $PT = 45.0$ mm and the longitudinal pitch is set to $PL = 22.5$ mm. The Reynolds number based on the tube diameter and the average entrance velocity $V_0 = 1.06$ m/s

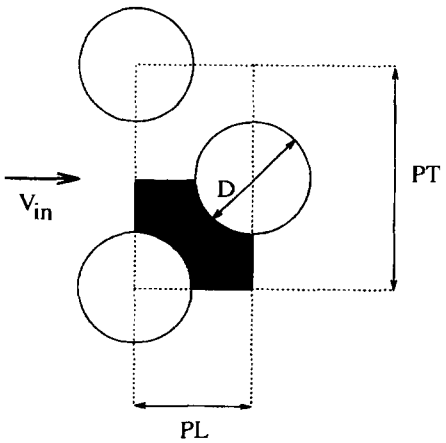

Fig. 3. Staggered tube bank geometry.

is given as 18,000. Due to the incompressibility constraint, the average inlet velocity equals $PT/(PT-D)V_0 = 1.93V_0$. However, experiments suggest that $V_{in} = 1.55V_0$, which implies that the flow rate at the inlet is about $Q = 0.02\ \mathrm{m}^2/\mathrm{s}$.

As mentioned before, after several rows of tubes the flow becomes periodic and the computation can be reduced to a minimal inter-tube space using symmetry and anti-periodic inlet/outlet conditions. It is assumed that at planes of symmetry the tangential stress and normal velocity are both zero, whereas for turbulence quantities homogeneous Neumann boundary conditions are imposed. The wall functions are applied at curved smooth walls. Anti-symmetrical periodic conditions as described in [28] are employed at the sections $X = 0$ mm and $X = 22.5$ mm. Here, the velocity components and turbulence quantities as well as geometrical quantities are adapted to the periodicity in anti-symmetrical manner. Furthermore, in order to have a flow, the pressure at $X = 22.5$ mm differs an unknown constant from the pressure at $X = 0$ mm. This constant can be determined from the imposed flow rate Q at $X = 0$. In fact, this constant can be considered as a Lagrange multiplier that enforced an overall mass balance. It is thus natural to extend the pressure correction method with this additional constraint in order to "correct" the pressure such that the velocity field satisfy overall continuity. For time discretization the implicit Euler scheme ($\theta = 1$) has been selected.

The grid employed in the computations is given in Fig. 4. The number of grid points is 80×32. Grid dependence test were performed with three different grids: 30×20, 55×28 and 80×32 cells. To ensure that the computational points near the tube walls have a non-dimensional wall distance of $Y^+ > 11$, no more than about 30 grid points in Y-direction were taken. The results of the test are presented in Fig. 5 where the wall shear stress (which is very sensitive) around one half of the tube is plotted for different grids (where α is the angle measured from the front stagnation point). There is very little difference between the two finest grids. Hence, it may be concluded that fully

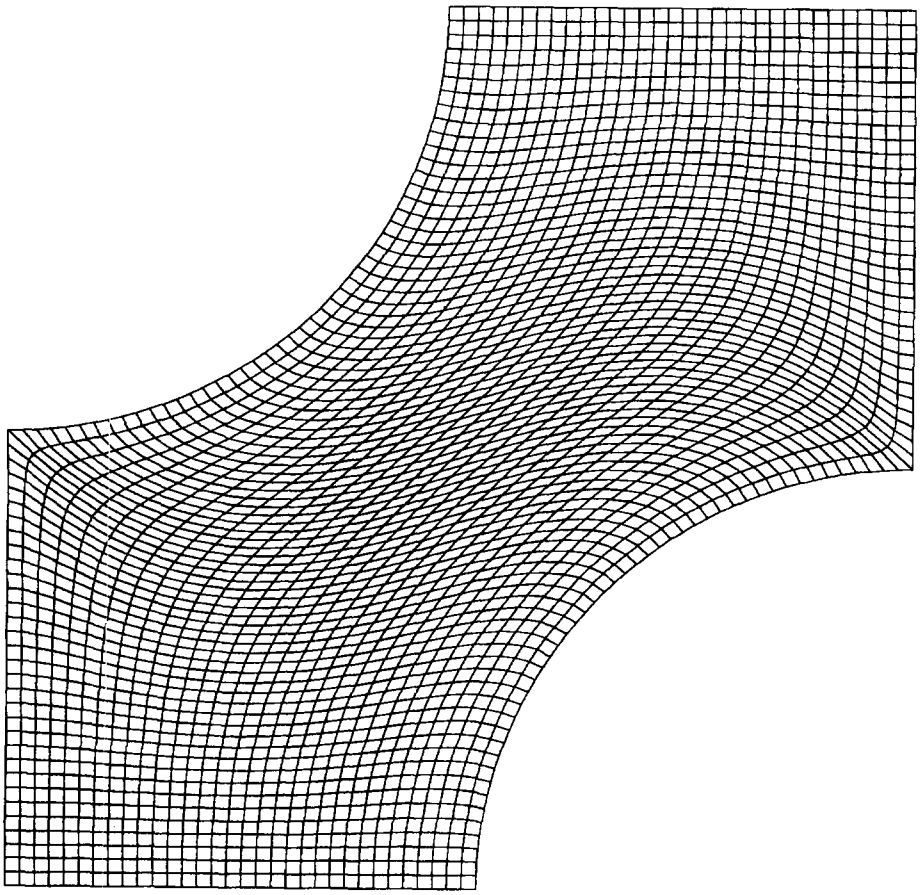

Fig. 4. A 80×32 grid for the flow through a tube bank sub-channel.

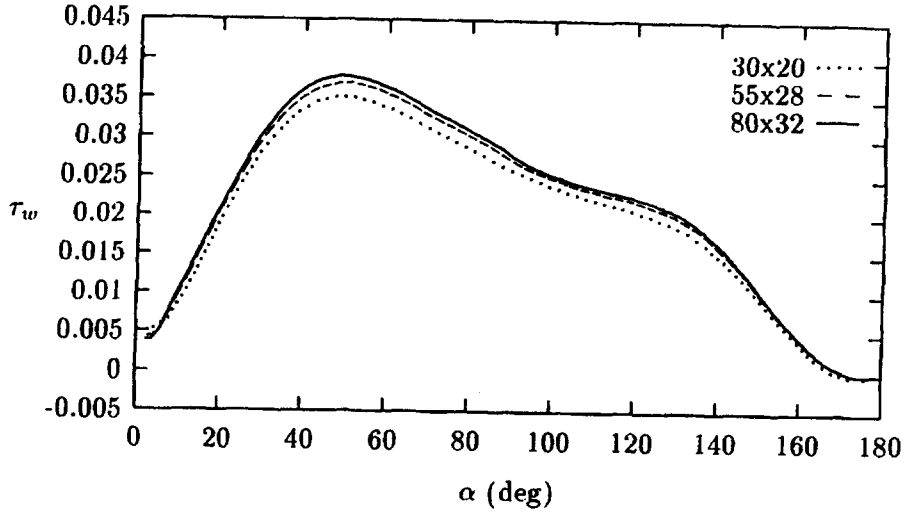

Fig. 5. Grid dependence test.

grid-independent solutions are nearly achieved on the 80 × 32 grid and thus will be presented in further detail below. The calculations on the 80 × 32 grid took 115 time steps ($\Delta t = 0.001$ s) and consumed 8 CPU minutes on a HP 9000/735 workstation. Here, the momentum and turbulence equations are solved with the GMRES method combined with an ILUD preconditioner, whereas the pressure system is solved with the GMRES method postconditioned by an ILU factorization. As stopping criterion the inequality $\|r\|_2/\|r_0\|_2 < 10^{-3}$ is used for the momentum and turbulence equations, while $\|r\|_2/\|r_0\|_2 < 10^{-4}$ is used for the pressure system. Here, r_0 and r are the initial residual norm and a given residual norm, respectively.

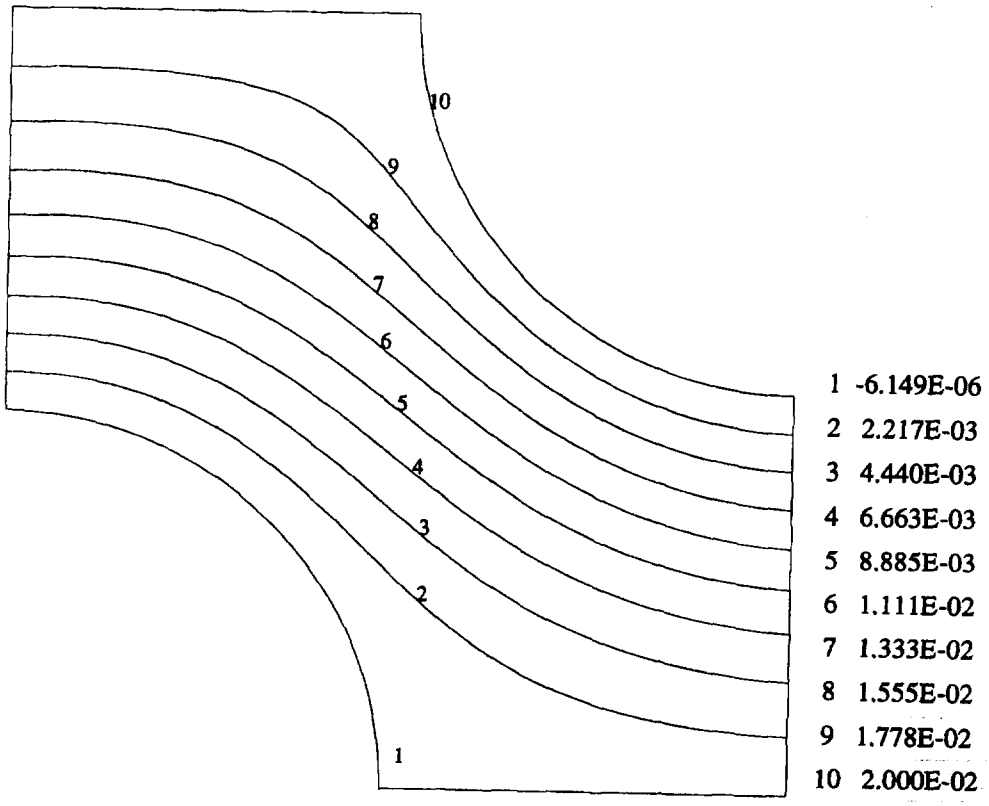

Fig. 6. Streamlines for flow across staggered tube bank.

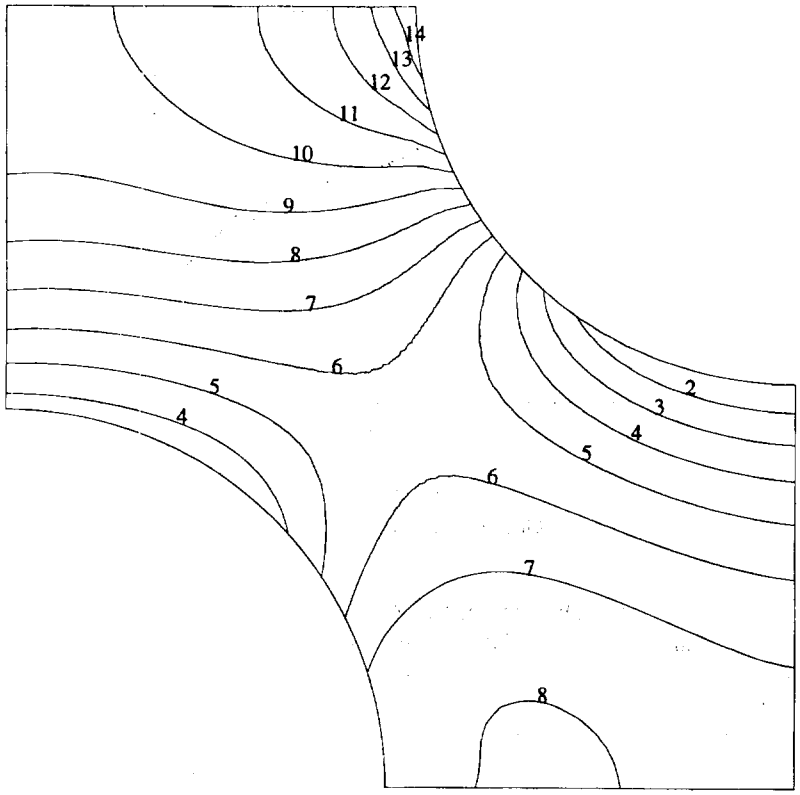

Fig. 7. Isobars for flow across staggered tube bank.

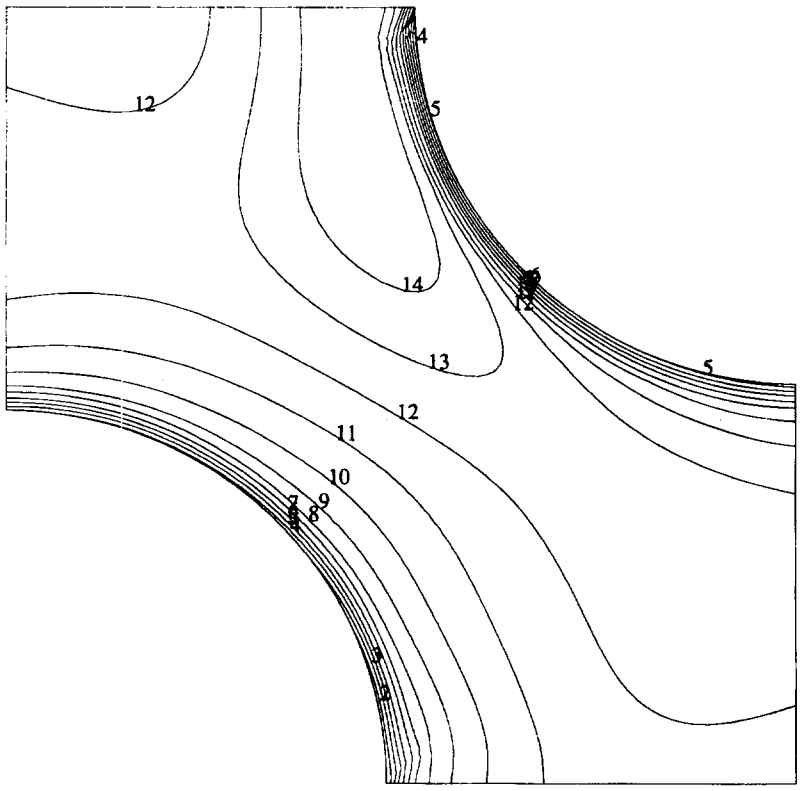

Fig. 8. Turbulence intensity $\sqrt{k}/V_0$ for flow across staggered tube bank.

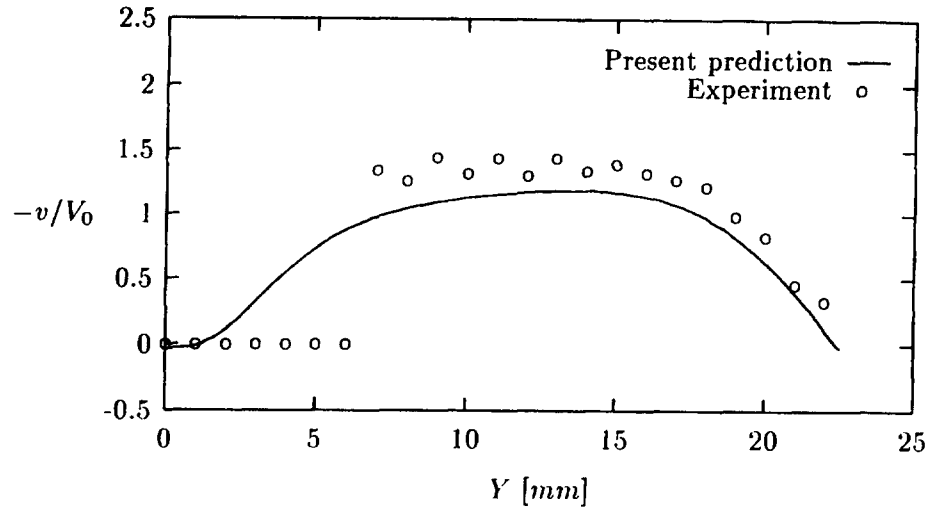

Fig. 9. Crosswise velocity profile at $X = 11$ mm.

Contour plots of streamlines, isobars and turbulence intensity (defined as $\sqrt{k}/V_0$) are shown in Figs 6, 7 and 8. They show clearly the increase of pressure as the flow approaches the impingement region and the steep gradients of turbulence levels near the tube. Furthermore, the standard k–ϵ model inhibits separation and is expected to overestimate the levels of turbulent energy at impingement zones, because of a misrepresentation of strain effects when the exact production terms are modeled with the isotropic eddy-viscosity concept. Also the turbulence levels in the wake behind the tube are assumed to be rather underestimated.

Comparisons with the experiments are shown in Figs 9–12. These figures represent the normalized velocity and turbulent stresses profiles along $X = 11$ mm (across the recirculation region behind the lower tube and the impingement region in front of the upper tube) and $Y = 22.5$ mm (along upper plane of symmetry), respectively.

It is seen that the standard k–ϵ model does not produce a significant recirculation zone and generates excessive levels of turbulent energy (in particular the streamwise normal stress component $\overline{u'^2}/V_0^2$) at the impingement zone.

The qualitative trends are well resolved by the present method. The mean velocity profiles are generally better predicted than turbulent stresses. According to the Workshop, the same conclusion can be drawn for other turbulence models, including the Reynolds-stress type. Furthermore, the agreement between the present predictions and the results of other contributors of the Workshop using the same models can be said to be satisfactory.

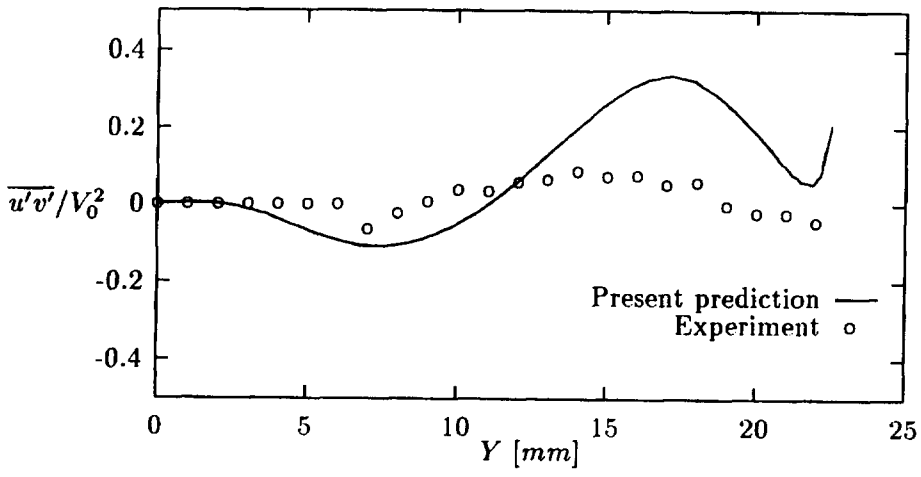

Fig. 10. Shear stress profile at $X = 11$ mm.

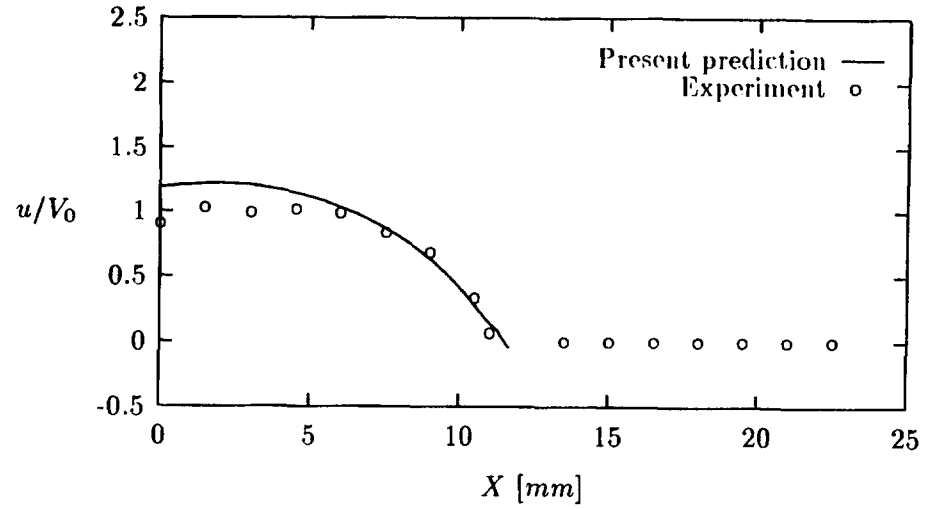

Fig. 11. Streamwise velocity profile at $Y = 22.5$ mm.

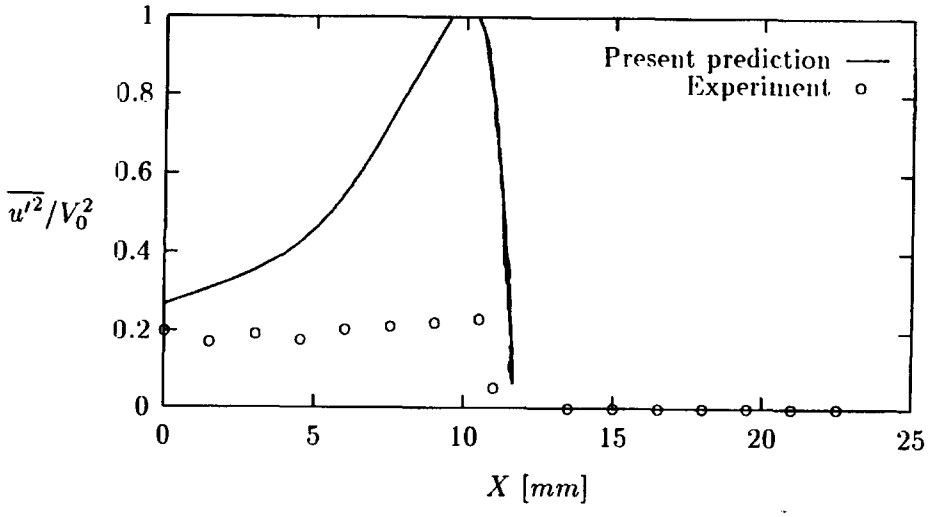

Fig. 12. Streamwise normal stress profile at $Y = 22.5$ mm.

6. CONCLUSIONS

An invariant formulation and discretization in general co-ordinates of the high-Re k–ϵ model including boundary conditions has been presented. Furthermore, it has been shown that if the k–ϵ model has a smooth solution for given positive initial conditions, positive Dirichlet and homogeneous Neumann boundary conditions, then k and ϵ stay positive at all times.

An important desirable property of a difference scheme for the k–ϵ model is positiveness, implying that physically non-negative turbulence quantities are never negative numerically. For highly convective turbulent flows in non-orthogonal grids, care must be taken in discretizing k–ϵ equations. For that reason the convection term is approximated with a second-order TVD/MUSCL scheme, whereas the mixed derivatives in diffusion terms should be approximated according to (32) and (33) or (35) and (36), in the case of highly non-orthogonal grids. Otherwise, to keep false diffusion to a minimum, equation (31) is appropriate as a differencing scheme for the mixed derivatives.

For time discretization the θ-method has been applied. Linearization of the nonlinear system of equations has been carried out with standard Newton method, which is found to avoid negative coefficients in the scheme. The resulting linear systems of equations are solved with a GMRES-type iterative method with preconditioning.

The tube bank case has demonstrated the capabilities of the numerical method to handle problems in which both the geometry and the flow are complicated. Predictions for the tube bank are found to compare well qualitatively with experimental data. However, appreciable differences between the predictions and data has been observed, probably due to weaknesses of the k–ϵ model.

REFERENCES

1. S. B. Pope, The calculation of turbulent recirculating flows in general orthogonal coordinates. *J. Comput. Phys.* **26,** 197 (1978).
2. I. Demirdzic, A. D. Gosman, R. I. Issa and M. Perić, A calculation procedure for turbulent flow in complex geometries. *Computers Fluids* **15,** 251 (1987).
3. H. C. Chen, V. C. Patel and S. Ju, Solutions of Reynolds-averaged Navier–Stokes equations for three-dimensional incompressible flows. *J. Comput. Phys.* **88,** 305 (1990).
4. M. C. Melaaen, Analysis of fluid flow in constricted tubes and ducts using body-fitted non-staggered grids. *Int. J. Numer. Meth. Fluids* **15,** 895 (1991).
5. P. J. Coelho and J. C. F. Pereira, Finite volume computation of the turbulent flow over a hill employing 2D or 3D non-orthogonal collocated grid systems. *Int. J. Numer. Meth. Fluids* **14,** 423 (1992).
6. W. Rodi, S. Majumdar and B. Schönung, Finite volume methods for two-dimensional incompressible flows with complex boundaries. *Comput. Meth. Appl. Mech. Engng* **75,** 369 (1989).
7. A. E. Mynett, P. Wesseling, A. Segal and C. G. M. Kassels, The ISNaS incompressible Navier–Stokes solver: invariant discretization. *Appl. Sci. Res.* **48,** 175 (1991).
8. P. Wesseling, A. Segal, J. J. I. M. van Kan, C. W. Oosterlee and C. G. M. Kassels, Finite volume discretization of the incompressible Navier–Stokes equations in general coordinates on staggered grids. *Comput. Fluid Dyn. J.* **1,** 27 (1992).
9. A. Segal, P. Wesseling, J. van Kan, C. W. Oosterlee and K. Kassels, Invariant discretization of the incompressible Navier–Stokes equations in boundary fitted co-ordinates. *Int. J. Numer. Meth. Fluids* **15,** 411 (1992).
10. C. W. Oosterlee and P. Wesseling, A robust multigrid method for a discretization of the incompressible Navier–Stokes equations in general coordinates. *Impact Comput. Sci. Engng* **5,** 128 (1993).
11. B. E. Launder and D. B. Spalding, The numerical computation of turbulent flows. *Comput. Meth. Appl. Mech. Engng* **3,** 269 (1974).
12. I. A. Demirdzic, A finite volume method for computation of fluid flow in complex geometries. Ph.D. thesis, University of London (1982).
13. C. M. Rhie and W. L. Chow, Numerical study of the turbulent flow past an airfoil with trailing edge separation. *AIAA J.* **21,** 1525 (1983).
14. M. Perić, Finite volume method for the prediction of three-dimensional fluid flow in complex ducts. Ph.D. thesis, Imperial College, London (1985).
15. F.-S. Lien and M. A. Leschziner, Multigrid convergence acceleration for complex flow including turbulence. In *Multigrid Methods III* (Edited by W. Hackbush and U. Trottenberg), Vol. 98, pp. 277–288. Birkhäuser, Basel (1991).
16. N.-H. Cho and C. A. J. Fletcher, Computation of turbulent conical diffuser flows using a non-orthogonal grid system. *Computers Fluids* **19,** 347 (1991).
17. R. Aris, *Vectors, Tensors and the Basic Equations of Fluid Mechanics.* Prentice-Hall, Englewood Cliffs, N.J. (1962).
18. I. S. Sokolnikoff, *Tensor Analysis.* Wiley, Englewood Cliffs, N.J. (1964).
19. B. Cardot, B. Mohammadi and O. Pironneau, A few tools for turbulence models in Navier-Stokes equations. In *Incompressible Computational Fluid Dynamics* (Edited by M. D. Gunzburger and R. A. Nicolaides), pp. 1–15. Cambridge Univ. Press, Cambridge, U.K. (1993).
20. S. V. Patankar and D. B. Spalding, A calculation procedure for heat, mass and momentum transfer in three-dimensional parabolic flow. *Int. J. Heat Mass Transfer* **15,** 1787 (1972).
21. M. A. Leschziner, Modeling turbulent recirculating flows by finite-volume methods—current status and future directions. *Int. J. Heat Fluid Flow* **10,** 186 (1989).
22. C. Hirsch, *Numerical Computation of Internal and External Flows,* Vols. 1 and 2. Wiley, Chichester (1990).
23. Y. Saad and M. H. Schultz, GMRES: a generalized minimal residual algorithm for solving non symmetric linear systems. *SIAM J. Sci. Stat. Comput.* **7,** 856 (1986).
24. C. Vuik, Solution of the discretized incompressible Navier–Stokes equations with the GMRES method. *Int. J. Numer. Meth. Fluids* **16,** 507 (1993).
25. J. J. I. M. van Kan, A second-order accurate pressure correction method for viscous incompressible flow. *SIAM J. Sci. Stat. Comput.* **7,** 870 (1986).
26. D. Simonin and M. Barcouda, Measurements and predictions of turbulent flow entering a staggered tube bundle. EDF Report H-44/88.25, EDF, Laboratoire National d'Hydraulique, Chatou, France (1988).
27. M. A. Leschziner and B. E. Launder (Eds), *Round normally impinging turbulent jet and turbulent flow through tube bank sub-channel,* Manchester, U.K. UMIST. Proc. Second ERCOFTAC-IAHR Workshop on Refined Flow Modelling (1993).
28. G. Segal, K. Vuik and K. Kassels, On the implementation of symmetric and antisymmetric periodic boundary conditions for incompressible flow. *Int. J. Numer. Meth. Fluids* **18,** 1153 (1994).

APPENDIX

Theorem

If the initial and the Dirichlet conditions for $\Theta = k/\epsilon$ are positive, the normal gradient of Θ is zero at Neumann boundaries and $c_{\epsilon 2} > 1$ then

$$\forall t \geqslant 0: \quad \Theta > 0$$

For the proof of this theorem we need an equation for Θ. Equations (14) and (15) can be combined to yield the following equation

$$\frac{\partial \Theta}{\partial t} + (U^{\alpha}\Theta)_{,\alpha} = 2c_{\mu}\Theta^2 S^{\alpha\beta}S_{\alpha\beta}(1 - c_{\epsilon 1}) + c_{\epsilon 2} - 1 + g^{\alpha\beta}\frac{c_{\mu}}{\sigma_k}\Theta\frac{\partial\Theta}{\partial\xi^{\alpha}}\frac{\partial k}{\partial\xi^{\beta}} + 2g^{\alpha\beta}\frac{c_{\mu}}{\sigma_{\epsilon}}\Theta\frac{\partial k}{\partial\xi^{\alpha}}\frac{\partial\Theta}{\partial\xi^{\beta}}$$
$$- g^{\alpha\beta}\frac{c_{\mu}}{\sigma_{\epsilon}}k\frac{\partial\Theta}{\partial\xi^{\alpha}}\frac{\partial\Theta}{\partial\xi^{\beta}} + \frac{c_{\mu}}{\sigma_{\epsilon}}k\Theta(g^{\alpha\beta}\Theta_{,\beta})_{,\alpha} + \left(\frac{c_{\mu}}{\sigma_k} - \frac{c_{\mu}}{\sigma_{\epsilon}}\right)\Theta^2\left[(g^{\alpha\beta}k_{,\beta})_{,\alpha} + \frac{1}{k}g^{\alpha\beta}\frac{\partial k}{\partial\xi^{\alpha}}\frac{\partial k}{\partial\xi^{\beta}}\right] \quad \text{(A1)}$$

where

$$S^{\alpha\beta} = \tfrac{1}{2}(g^{\alpha\gamma}U^{\beta}_{,\gamma} + g^{\beta\gamma}U^{\alpha}_{,\gamma}), \quad S_{\alpha\beta} = \tfrac{1}{2}(U_{\alpha,\beta} + U_{\beta,\alpha}) \quad \text{(A2)}$$

are the contravariant and covariant components of the mean rate of strain tensor, respectively.

Proof of the Above Theorem

By contradiction. Let t_0 be the first time that there exists a $\xi \in G$ such that $\Theta(\xi, t_0) = 0$. Since $\Theta(\xi, t) \geqslant 0$ for $t \leqslant t_0$,

$$\frac{\partial\Theta}{\partial t} \leqslant 0 \quad \text{at } t = t_0 \quad \text{(A3)}$$

Because we have a minimum, at (ξ, t_0) with $\xi \in G\backslash\partial G_D$ the gradient of Θ is zero; this holds also at Neumann boundaries because of the homogeneous Neumann condition. Thus, equation (A1) reduces to $\partial\Theta/\partial t = c_{\epsilon 2} - 1 > 0$. This inequality contradicts the inequality (A3) and we conclude that $\forall t \geqslant 0$: $\Theta > 0$. □